Published in Journal of Electronic Materials, 43, 2984-2990 (2014)

MODELING InAs/GaSb AND InAs/InAsSb SUPERLATTICE INFRARED DETECTORS

P.C. Klipstein*, Y. Livneh+ , A. Glozman, S. Grossman, O. Klin, N. Snapi, E. Weiss

SemiConductor Devices, P O Box 2250, Haifa 31021, Israel

+ Department of Physical Electronics, Tel-Aviv Univ., Tel-Aviv 69978, Israel

ABSTRACT

InAs/GaSb and InAs/InAsSb type II superlattices have been proposed as promising alternatives to HgCdTe for the photon absorbing layer of an infrared detector. When combined with a barrier layer based on an InAs/AlSb superlattice or a AlSbAs alloy, respectively, they can be used to make diffusion limited "barrier" detectors with very low dark currents. In this work we compare theoretical simulations with experimental bandgap and photoabsorption data for such superlattices, spanning from the mid- to the long-wave infra-red (2.3-12 μm). The spectral response of detectors based on these materials is also simulated. The simulations are based on a version of the $\mathbf{k} \cdot \mathbf{p}$ model developed by one of the authors, which takes interface contributions and bandgap bowing into account. Our results provide a way of assessing the relative merits of InAs/GaSb and InAs/InAsSb superlattices as potential detector materials.

Key Words: Infrared detector, XBn, pBp, Type II superlattice, Gallium free superlattice, $\mathbf{k} \cdot \mathbf{p}$ method

INTRODUCTION

Over the last few years, InAs/GaSb type II superlattices (T2SLs) have attracted attention as a promising III-V alternative to HgCdTe for infrared detector applications [1]. Recently it was proposed that InAs/InAsSb Ga-free T2SLs may offer superior performance due to their longer carrier lifetime [2]. In this work we

* Tel: (972)-4-990-2559; Fax: (972)-4-990-2686; *Email*: philip_k@scd.co.il

compare theoretical simulations with experimental bandgap data for more than 30 InAs/GaSb T2SLs grown by molecular beam epitaxy (MBE) with "InSb-like" interfaces and with cut-off wavelengths from the mid-wave infra-red (MWIR) to the long-wave infra-red (LWIR). We also address the optical properties of two other T2SL structures which are lattice matched to a GaSb substrate: InAs/AlSb and InAs/InAsSb. The simulations are based on a modified version of the $\mathbf{k} \cdot \mathbf{p}$ model with a small number of input parameters [3]. This model was developed by one of the authors after Takhtamirov and Volkov [4] showed that the widely used Burt-Foreman approach is incomplete. Some notable points in the model are [5,6]:

(1) An interface matrix which is essentially diagonal in the case of no common atom (NCA) superlattices such as InAs/GaSb or InAs/AlSb and which has three leading parameters: D_S, D_X and D_Z.

(2) An interface matrix which is essentially off-diagonal for common atom (CA) superlattices such as GaSb/AlSb or InAs/InAsSb and which has two leading parameters, α and β.

(3) A reduction in the number of independent Luttinger parameters. Namely, using equation C1 of Ref. 5, four out of the six Luttinger parameters (three for each material) can be expressed in terms of the other two, with no loss of precision. This provides a direct way of determining all three parameters in the alloy layer of an InAs/InAsSb T2SL. It should be noted that standard methods of interpolation do not work for the alloy, due to strong bowing effects.

In the next three sections we present a comparison between experimental bandgap data and theoretical simulations for three types of InAs/X superlattice (X=GaSb, AlSb or InAsSb). The data is in the form of low temperature photoluminescence or absorption spectra (see Ref. 5 for details of the methods of measurement). We then compare the simulated performance of LWIR detectors based on InAs/GaSb and InAs/InAsSb T2SL photon absorbing layers, respectively. Note that all T2SL layer thicknesses are given in monolayers (ML).

InAs/GaSb TYPE II SUPERLATTICES

Figure 1 shows a comparison between the calculated bandgaps and the photoluminescence (PL) peak energies measured at 10K for our set of InAs/GaSb T2SLs. The calculations were based on InAs and GaSb layer widths determined with a typical accuracy of ±0.2 ML, by finding a single pair of growth constants for more than 30 T2SLs, which when multiplied by the beam fluxes and shutter timings gave the least RMS errors

for the precisely measured superlattice periods [5]. The measured and calculated energies in Figure 1 match the ideal behavior (thick line) to within an accuracy of $\pm k_B T$ at 77K (thin lines), for bandgap energies between 100 to 300meV (cut-off wavelengths between 4 and 12 μm). Figure 2 shows examples of measured (grey) and calculated (black) absorption spectra for MWIR and LWIR T2SL structures. All of the main features in the measured spectra are reproduced, including the strong peak due to the zone boundary $HH_2 \rightarrow E_1$ transition below 3 μm [5]. Note that this peak is much stronger than the longer wavelength zone centre $LH_1 \rightarrow E_1$ transition (at ~3.4 μm in Figure 2 (a)), because it has a larger oscillator strength and because the in-plane HH_2 energy dispersion is electron like at small wave-vector, leading to a very high joint density of states. In fact, the $LH_1 \rightarrow E_1$ transition does not show a clear peak in our calculation, because we use a simple linear increase of the inhomogeneous broadening with energy [5] which probably over broadens this particular transition. Our two independent Luttinger parameters are γ_1 and γ_2 for InAs, and they have fitted values of 19.77 and 8.57 respectively. The fitting procedure involves finding a single set of two Luttinger parameters, three interface parameters, and the valence band offset, that give the best fits to the absorption spectra and bandgap energy data shown in Figures 1 and 2. Further details of the fitting procedure may be found in Ref. [5]. The values of γ_1 and γ_2 for InAs, and those of the four remaining Luttinger parameters calculated from them (γ_3 for InAs, and γ_1, γ_2, γ_3 for GaSb), are all within 3% of those proposed by Lawaetz [7]. The other fitted parameter values are the interface potentials: D_S, D_X, D_Z = −1.70, 1.17, −1.17 eV Å, and the valence band offset: VBO = −0.553eV (with respect to the valence band of GaSb). The matrix element scaling parameter defined in Ref. 5, although not needed to fit the energies, was η=1.13 ± 0.09 [8]. It should be noted that if we omit the interface matrix, the calculated bandgaps in Figure 2 exhibit a blue-shift of about 0.75 μm for the MWIR T2SL and 4.5 μm for the LWIR T2SL. This demonstrates that the contribution of the interface potentials to the superlattice bandstructure is far from negligible.

We have also tested our model against experimental data on other InAs based superlattice structures, namely InAs/AlSb and InAs/InAsSb and it works remarkably well. In each case we use the same values of γ_1 and γ_2 for InAs (19.77 and 8.57) and do not need to introduce any other independent Luttinger parameters. In the next section, we show results for InAs/AlSb T2SLs. These superlattices are important because they can be

used as the barrier material in a XBp barrier detector structure made with an InAs/GaSb T2SL photon absorbing active layer (AL). Results for InAs/InAsSb T2SLs are then presented in the following section.

InAs/AlSb SUPERLATTICES

Figure 3 shows that within the range of experimental error, the calculated bandgaps of fourteen InAs/AlSb T2SLs with "InSb-like" interfaces agree quite well with the measured values for bandgap energies between 350 and 530 meV (cut-off wavelengths between 2.3 and 3.5 μm). In some cases not all of the individual layer thicknesses could be determined to an accuracy of ±0.2 ML, and for these cases the resulting energy uncertainty is indicated with error bars. The largest thickness uncertainty was ±0.5 ML. The following values were used for the interface parameters: D_S, D_X, D_Z = –0.8, 2.4, –0.5 eV Å, and the InAs valence band was 109 meV below that of AlSb [9].

InAs/InAsSb GALLIUM FREE SUPERLATTICES

Figure 4 shows a comparison between measured and calculated absorption spectra for a 12.8/12.8 $InAs/InAs_{0.815}Sb_{0.185}$ T2SL. Note that all the main features of the experimental spectrum in Figure 4 are reproduced by our calculation, including the bandgap, the strength of the absorption, and the wavelengths of the four points where the slope changes abruptly.

Since the composition difference between the two layers in this CA superlattice is less than 20%, the two interface parameters, α and β, are reduced by more than 80% and can be taken to be negligibly small. There are no other interface parameters in a CA superlattice. The interface matrix can therefore be neglected and the calculation is a simple piecewise calculation based on bulk matrices for InAs and the InAsSb alloy. The parameters which were fitted in this calculation, in order to get the good agreement between model and experiment in Figure 4, are the bowing parameters in the alloy for the bandgap, E_0, and for the VBO. As described below the former has a strong influence on the values which we calculate for the Luttinger parameters of the alloy, while the latter affects the optical transition energies between the various mini-bands in the superlattice. If we express any physical property of the $InAs_{1-x}Sb_x$ alloy, such as the bandgap or VBO, by the general expression $Y = Y(\text{InAs}) + \{Y(\text{InSb}) - Y(\text{InAs})\}.\, x + \{C_1 + C_2.\, x\}x(1-x)$, then the following values

(in eV) were found to give a reasonably good fit to our absorption data and to the low temperature PL data recently reported by Lin et al. [10] for InAs/InAsSb T2SLs and bulk layers with Sb-concentrations of up to ~40%: (C_1, C_2) = (1.08, -0.42) for the bandgap, and (C_1, C_2) = (-0.21, 0) for the VBO. Bowing parameters of (C_1, C_2) = (0.0456, 0) and (1.05 eV, 0) were also used for the conduction band effective mass ratio, m_c^*/m_0 (where m_0 is the free electron mass), and the spin-orbit splitting, Δ_0, based on data in Ref. 11. Linear interpolation was used for the bandgap energies E_0', Δ_0' and for the $\mathbf{k} \cdot \mathbf{p}$ parameter, E_P (notation as in Ref. 5). This was also based on data in Ref. 11 for the two bandgaps, and on a 5-level $\mathbf{k} \cdot \mathbf{p}$ analysis [6] for E_P. The matrix element scaling parameter was found to be $\eta = 0.99$. Presumably it is closer to unity than in the case of an InAs/GaSb T2SL, because the two superlattice materials are rather more similar to one another.

It was mentioned in the Introduction that we calculate the Luttinger parameters for the alloy from the values of γ_1 and γ_2 for InAs and equations C1 in Ref. 5. The results depend on the choice of bowing parameters for E_0, Δ_0, E_0', Δ_0' and E_P. Of these, the first two are the most critical, while the other three have a much weaker effect. Figure 5 (a) shows the values of γ_1 and γ_2 in the alloy and also the difference between γ_3 and γ_2, for our final choice of bowing parameters quoted above. It can be seen that the bowing effect is extremely strong in all three of the alloy Luttinger parameters. The values calculated for an alloy composition of x=1 (corresponding to InSb) are all within 2% of the Lawaetz values [7]. This gives us a high level of confidence in the reliability of the Luttinger values for alloy compositions with $x < 1$. In Figure 5(b) we plot the light and heavy hole mass ratios along [100], m_{LH}/m_0 and $m_{HH}/m_0 = (\gamma_1 \pm 2\gamma_2)^{-1}$, which are calculated from the alloy Luttinger parameters in Figure 5(a). A popular way of estimating the Luttinger parameters of alloys [12] is to calculate them from linear interpolations of m_{LH}, m_{HH}, and γ_3 - γ_2. Figure 5 shows that while linear interpolation works reasonably well for the heavy hole mass and γ_3 - γ_2, it works very badly for the light hole mass. Therefore simple interpolation methods are not reliable in the presence of strong bandgap bowing.

SIMULATION OF SUPERLATTICE DETECTORS

InAs and As-rich InAsSb diodes are known to be very hard to passivate, due to a very strong accumulation layer that forms on exposed surfaces [13]. A more successful approach has been to use a new

XBn "barrier detector" architecture [14,15,16], which also reduces the dark current to that of MCT Rule 07 [17]. Recently InAs/InAsSb T2SLs have been proposed as a replacement for the lattice matched $InAs_{0.91}Sb_{0.09}$ alloy used in the AL of such XBn detectors grown on GaSb [18]. The cut-off wavelength can then be extended beyond ~4.2 µm, which is the wavelength of the lattice matched alloy and which lies roughly in the middle of the MWIR atmospheric transmission window. In order to investigate this approach, we have compared simulated spectral response curves of InAs/GaSb and InAs/InAsSb T2SL "barrier" detectors with a 10 µm bandgap wavelength. In barrier detectors, an important condition on the barrier is that it should block the flow of only one carrier type [16, 19]. Since the barrier material should also be closely lattice matched, this leads to the choice of an InAs/AlSb T2SL as the ideal barrier for a detector with an InAs/GaSb T2SL active layer. The detector is an XBp design because the barrier blocks the flow of holes but allows the more mobile electrons to flow freely. This is preferable to an XBn design, which can be made using a barrier such as GaAlSbAs alloy, because it ensures a larger minority carrier diffusion length. In the case of the detector with an InAs/InAsSb T2SL active layer, a lattice matched barrier only exists for the conduction band (AlSbAs alloy), leading to an XBn design. As will be discussed below, the low mobility of the minority carriers (holes) in this case is likely to limit the maximum quantum efficiency of the detector.

In order to simulate the spectral response of a superlattice barrier detector, we first calculate the absorption coefficient of the superlattice AL, as described above, and use it to determine the imaginary part of the complex refractive index. We then use a combination of the optical transfer matrix technique [20, 21] and the Van de Wiele model [22] to simulate the photoresponse. We assume a zero surface recombination velocity on the back side of the AL and average over different thicknesses of the thin remaining transparent GaSb substrate in order to suppress Fabry-Perot oscillations in the response curve. For simplicity we use the following values for the thickness (t) and the real part of the refractive index (n) in all cases: $t_{BL} = 0.5$µm, $t_{CL} = 0.2$ µm and $n_{AL} = n_{CL} = 3.6$, $n_{BL} = 3.4$ where CL and BL are the contact layer and barrier layer, respectively.

For a reasonable quantum efficiency (QE) in a strain balanced InAs/InAsSb T2SL grown on GaSb, a relatively high Sb concentration should be used, so that the T2SL period can be kept as small as possible. Figure 6 shows the calculated spectral response curves at 77K for double pass LWIR barrier detectors, each with a 5 µm AL thickness (t_{AL}) and with an antireflection coating (ARC) of optical thickness, 2.17 µm. The

two upper curves are for a 13.8/7 InAs/GaSb XBp structure [6] and a 31.5/9.5 InAs/ $InAs_{0.61}Sb_{0.39}$ XBn structure, respectively. Since the dispersion of the valence mini-band is very narrow, the results for the XBn case are shown as a function of the minority carrier diffusion length (L_D). Even when $L_D >> L_{AL}$, the QE of the XBn detector is significantly below that of the XBp, due to the smaller absorption coefficient of the InAs/InAsSb T2SL. It is in fact much more likely that $L_D < L_{AL}$, since very small hole mobility values have been reported recently from direct measurements on InAs/GaSb T2SL structures with a qualitatively similar valence band profile to that of the InAs/InAsSb T2SL considered here [23]. In Ref. 23 a vertical hole diffusion coefficient of 0.04 cm^2/s was reported at 77K for a 8/16 InAs/GaSb MWIR T2SL. For a typical minority carrier lifetime in MWIR InAs/GaSb of 65 ns [24], this corresponds to a diffusion length of only 0.5 μm. Moreover, when we calculate the valence band dispersion along the growth direction at zero and at small in-plane wave-vectors, for both the 8/16 InAs/GaSb T2SL of Ref. 23 and the InAs/InAsSb T2SL of Figure 6, the InAs/InAsSb T2SL exhibits the narrower dispersion. Therefore even though the InAs/InAsSb T2SL has a carrier lifetime typically about one order of magnitude greater than that in the InAs/GaSb T2SL [2], its narrower valence band dispersion will tend to compensate for any enhancement of the diffusion length due to the longer lifetime, so the vertical transport is unlikely to be significantly more effective in the InAs/InAsSb T2SL than in the InAs/GaSb T2SL. For these reasons we expect an upper limit on the diffusion length in the InAs/InAsSb T2SL of about 1 μm. The simulations in Figure 6 thus suggest that the maximum QE of the InAs/InAsSb XBn detector is not expected to exceed 10%. Even though the dark current in the InAs/InAsSb XBn detector is also expected to be very small due to a combination of the long carrier lifetime and the small diffusion length, the low QE will limit the value of such a detector in applications which require a high sensitivity or a high frame rate.

CONCLUSIONS

We have used a modified version of the $\mathbf{k} \cdot \mathbf{p}$ model to calculate the bandgaps and absorption spectra of three types of type II superlattice based on InAs, namely InAs/GaSb, InAs/AlSb and InAs/InAsSb. Important features of the model are different interface matrices for CA and NCA superlattices, and a reduction in the number of Luttinger parameters from the usual six to just two independent parameters. Using measured

bandgap data and γ_1 and γ_2 of InAs as the independent Luttinger parameters, it has previously been demonstrated that γ_3 of InAs and γ_1, γ_2 and γ_3 of the second superlattice material can all be determined with sufficiently high precision [5]. The two independent InAs parameters are evaluated by adjusting their values and the values of three interface parameters and the valence band offset, until a good fit is obtained with experimental InAs/GaSb T2SL absorption spectra in the MWIR and LWIR, and with bandgap wavelengths measured by low temperature PL on more than thirty T2SL structures spanning a range of 4 - 12 µm. In all these cases the individual InAs and GaSb layer thicknesses have been determined with a typical accuracy of 0.2 ML [5]. The PL bandgap wavelengths and all the main features of the absorption spectra are reproduced fairly well, including a strong peak in the absorption spectra due to the zone boundary $HH_2 \rightarrow E_1$ transition.

The two independent InAs Luttinger parameters deduced for the InAs/GaSb T2SLs were used without adjustment in the two other superlattice structures, InAs/AlSb and InAs/InAsSb. Most significantly, this approach provides a reliable way of calculating the three Luttinger parameters for the $InAs_{1-x}Sb_x$ alloy used in InAs/InAsSb T2SLs, even though it exhibits very strong bandgap bowing. Good agreement between our model and the experimental bandgap wavelengths determined from 10 K PL spectra was demonstrated for fourteen InAs/AlSb structures over a wavelength range of 2.3-3.5 µm. For a MWIR InAs/$InAs_{1-x}Sb_x$ T2SL ($x = 0.185$) the model was able to reproduce all of the main features of the experimentally measured absorption spectrum. In this case the bowing parameters of the fundamental bandgap and the VBO in $InAs_{1-x}Sb_x$ were deduced by adjusting their values until the best fit was obtained. Using the same bowing parameters we also found reasonable agreement between the model and measured bandgap data reported by Lin et al. [10] for bulk alloys and for five InAs/InAsSb T2SLs with x-values up to ~0.4. This will be reported in more detail in a future publication.

Having demonstrated that our model is able to provide a reasonably faithful simulation of the experimental absorption spectra for both InAs/GaSb and InAs/InAsSb T2SLs, we have used the simulated absorption spectra to calculate the two pass spectral response of an InAs/GaSb XBp detector and an InAs/InAsSb XBn detector, each with an active layer thickness of 5 µm and a cut-off wavelength close to 10 µm. It was noted that no suitable barrier material exists for the fabrication of an XBp design based on an InAs/InAsSb active layer. In the case of the InAs/InAsSb XBn detector, the response was calculated as a

function of the minority carrier diffusion length, since the diffusion length is expected to be smaller than the active layer thickness due to the absence of dispersion in the InAs/InAsSb valence band. Even for a very large diffusion length, the InAs/InAsSb T2SL has a significantly lower QE than the InAs/GaSb T2SL, due to its weaker absorption coefficient. When the short diffusion length is taken into account, the InAs/InAsSb XBn detector exhibits a much smaller QE (<10%) than the InAs/GaSb XBp detector (~70%). This may limit the value of the InAs/InAsSb XBn detector in LWIR applications which require a high sensitivity or a high frame rate.

ACKNOWLEDGEMENTS

We thank Dr. M. Katz and Mr. O. Westrich of the Soreq Research Centre for assistance with some of the PL measurements.

FIGURE CAPTIONS

FIGURE 1: (a) Comparison between calculated bandgaps and PL peak energies measured at 10K for more than 30 InAs/GaSb T2SLs spanning the MWIR to LWIR wavelength range. Thin lines show deviation by $\pm k_B T$ at 77 K from ideal behavior (thick line) (b) Expanded view of the LWIR region.

FIGURE 2: Measured (grey) and calculated (black) absorption spectra for (a) 8.4/13.7 MWIR and (b) 14.4/7.2 LWIR InAs/GaSb T2SLs (dimensions in ML). The large peaks at short wavelengths are from zone boundary $HH_2 \rightarrow E_1$ transitions.

FIGURE 3: Comparison between calculated bandgaps and PL peak energies measured at 10 K for 14 InAs/AlSb T2SLs.

FIGURE 4: Comparison between calculated (black) and measured (grey) absorption spectra for a 12.8/12.8 InAs/$InAs_{0.815}Sb_{0.185}$ T2SL at 77 K.

FIGURE 5: (a) Luttinger parameters at 77 K for $InAs_{1-x}Sb_x$ alloys, calculated from γ_1 and γ_2 of InAs using equation C1 or Ref. 5, and plotted as a function of alloy composition, x. (b) Heavy and light hole effective masses along the [100] direction, in units of the free electron mass, m_0, calculated from the values of γ_1 and γ_2 for $InAs_{1-x}Sb_x$ in (a).

FIGURE 6:

Calculated spectral response of a 13.8/7 InAs/GaSb XBp detector (red, solid) and a 31.5/9.5 InAs/$InAs_{1-x}Sb_x$ (x=0.39) XBn detector (blue, alternating solid and dash) at 77 K, as a function of the minority carrier diffusion length, L_D. In each case 80 % of the light is reflected back for a second pass, the ARC has an optical thickness of 2.17 μm, and the AL is 5μm.

FIGURES:

FIGURE 1

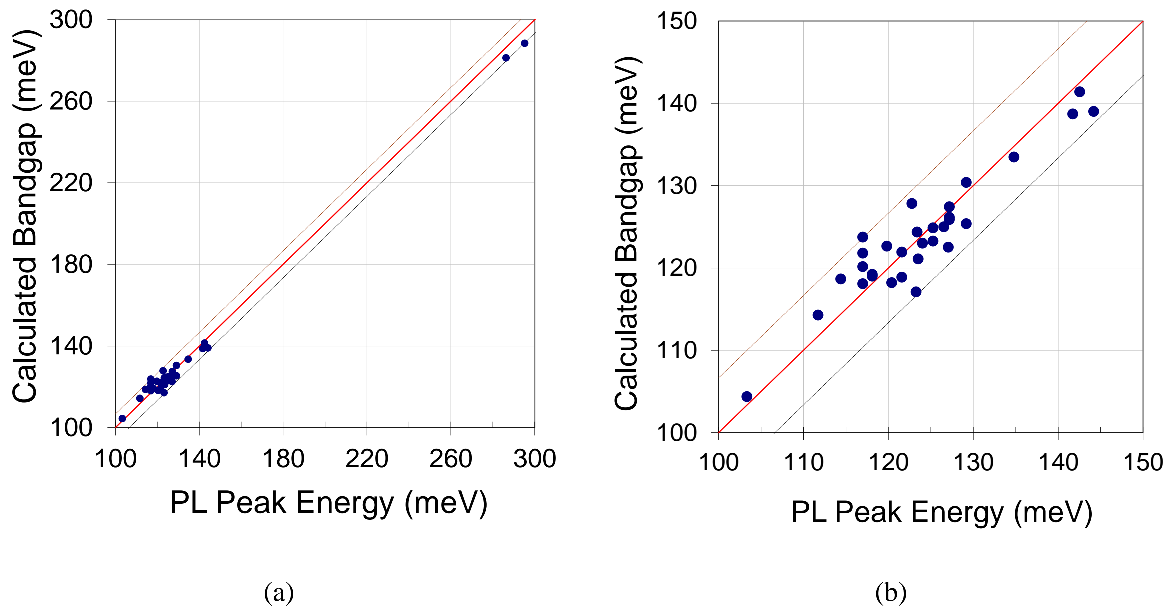

Figure 1

FIGURE 2

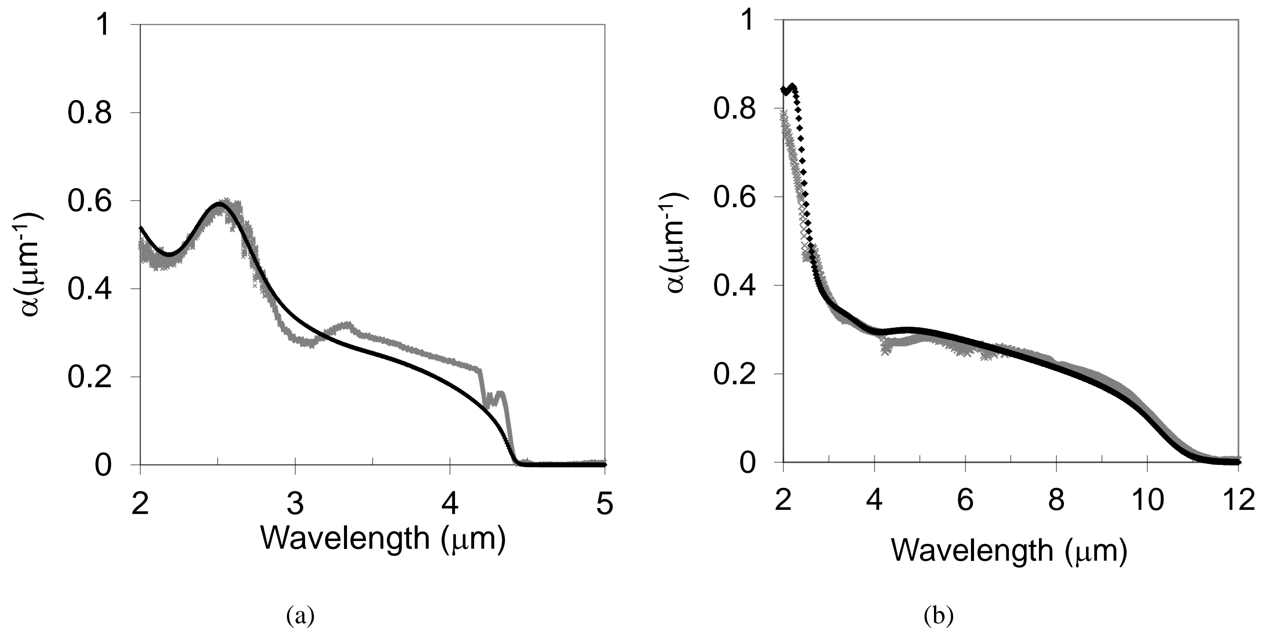

(a) (b)

Figure 2

FIGURE 3

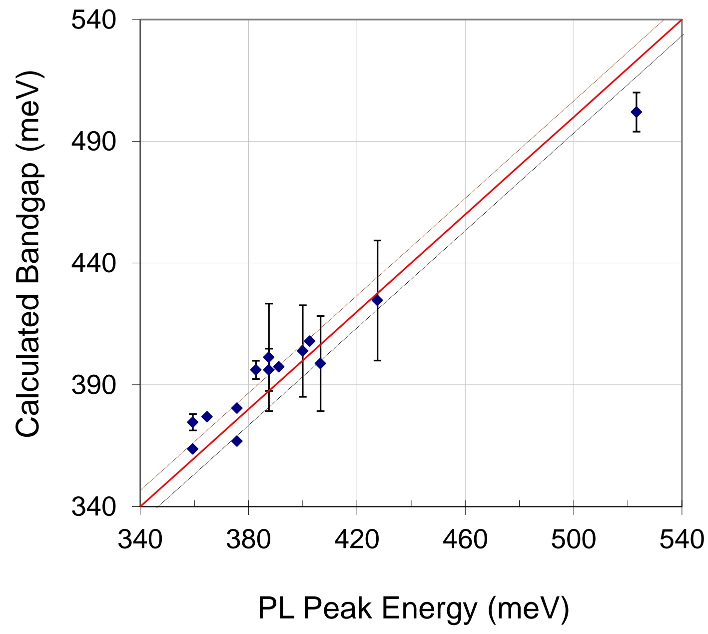

Figure 3

FIGURE 4

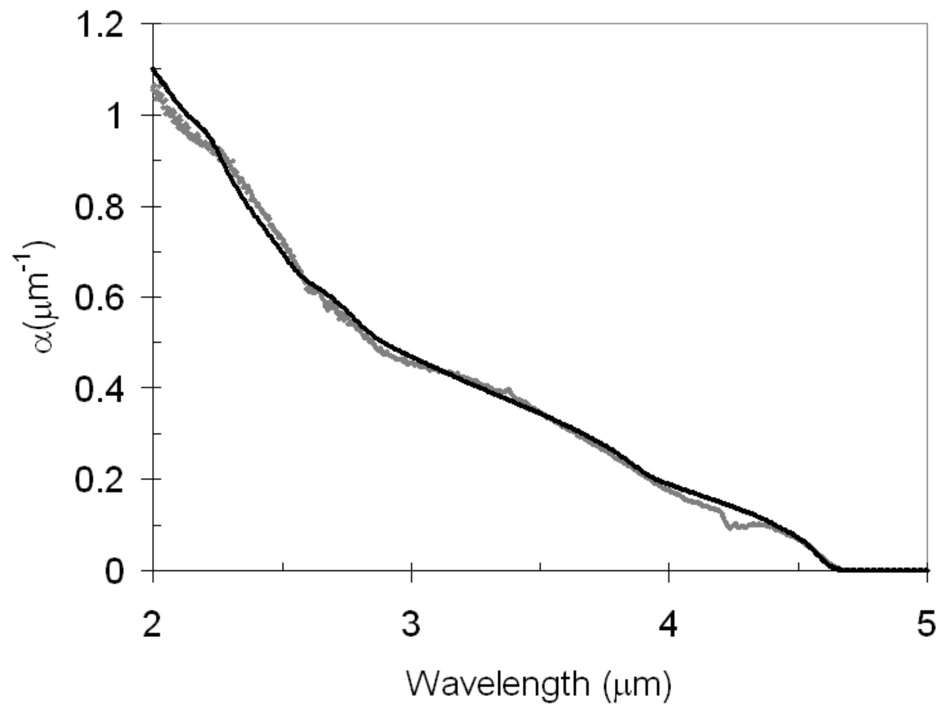

Figure 4

FIGURE 5

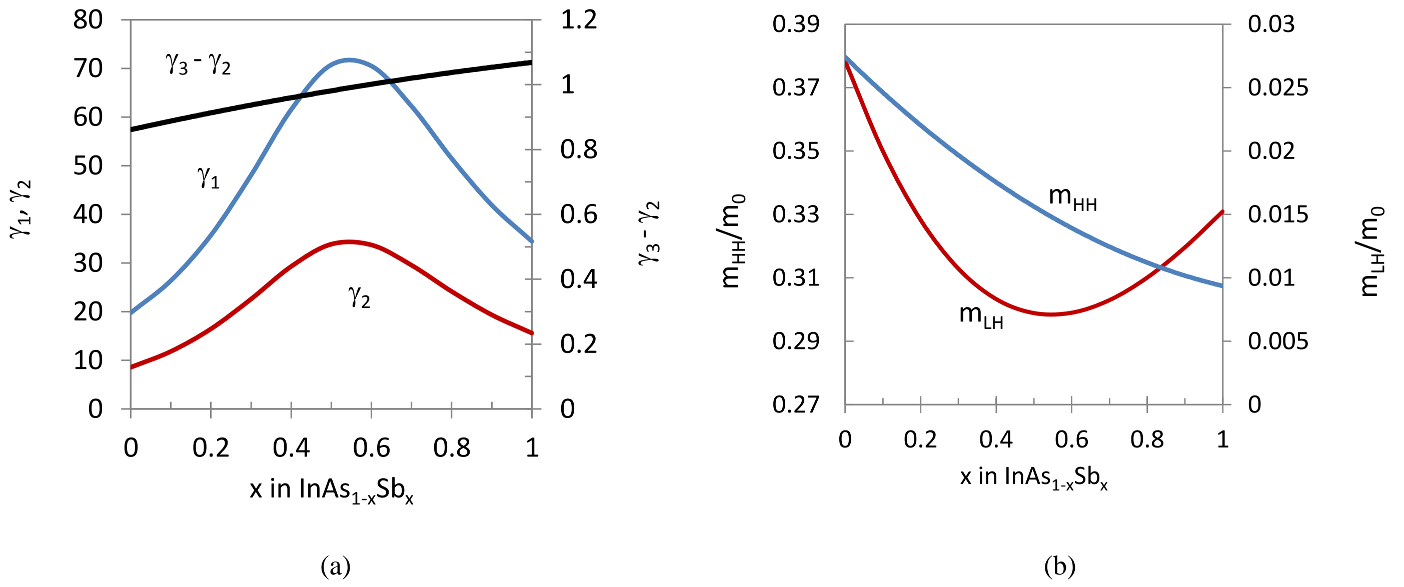

Figure 5

FIGURE 6

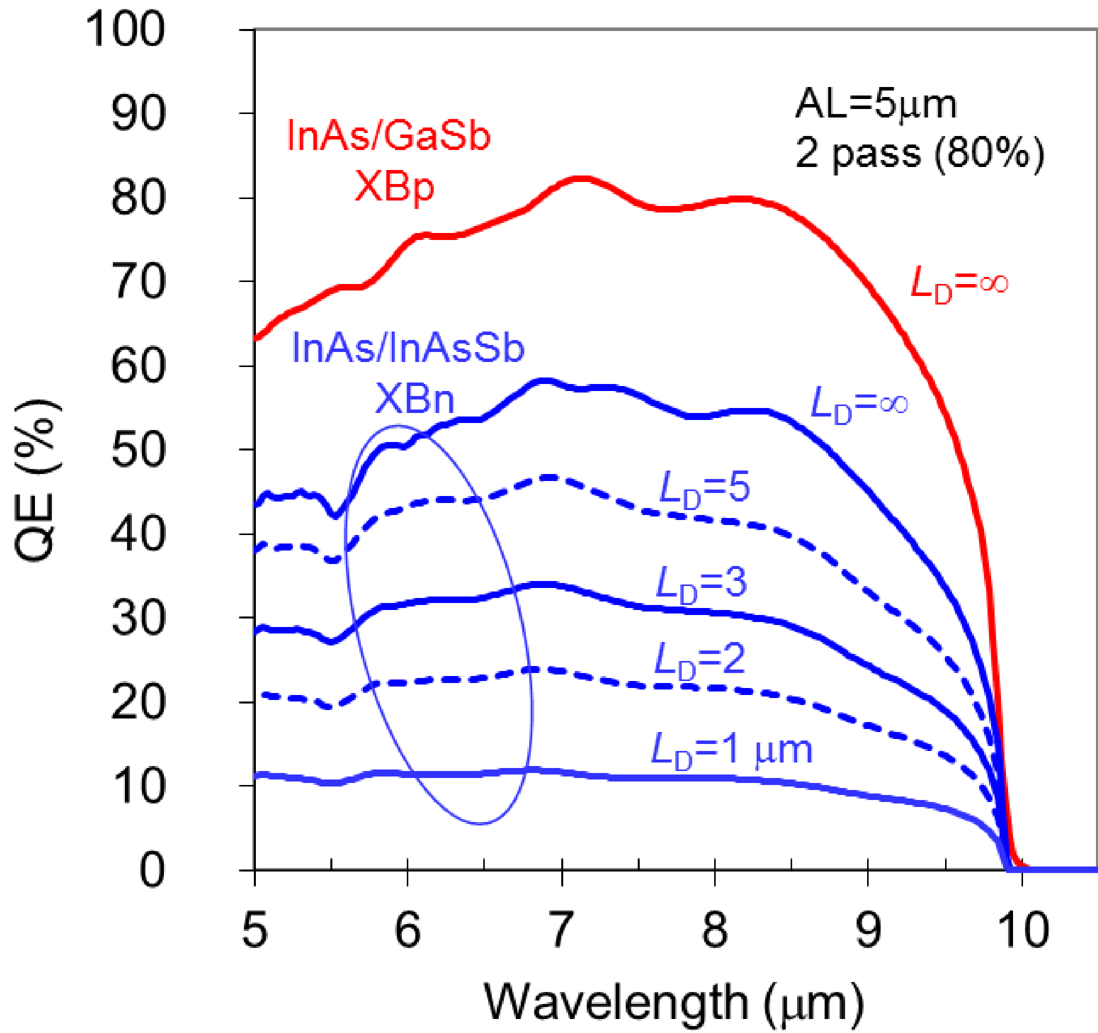

Figure 6

REFERENCES

[1] L. Bűrkle and F. Fuchs, "*Handbook of Infrared Detection Technologies"*, edited by M. Henini and M. Razeghi, p159; ibid. M. Razeghi and H. Mohseni, p 191 (Elsevier, UK, USA and Japan, 2002)

[2] E. H. Steenbergen, B. C. Connelly, G. D. Metcalfe, H. Shen, M. Wraback, D. Lubyshev, Y. Qiu, J. M. Fastenau, A. W. K. Liu, S. Elhamri, O. O. Cellek and Y.-H. Zhang., Appl. Phys. Lett. **99**, 251110 (2011)

[3] P.C. Klipstein, Phys. Rev. B **81**, 235314 (2010)

[4] E.E. Takhtamirov and V.A. Volkov , JETP **89**, 1000 (1999)

[5] Y. Livneh, P.C. Klipstein, O. Klin, N. Snapi, S. Grossman, A. Glozman, and E. Weiss, Phys. Rev. B **86**, 235311 (2012)

[6] P.C. Klipstein, Y. Livneh, O. Klin, S. Grossman, N. Snapi, A. Glozman, and E. Weiss, IR Physics and Technology **59**, 53 (2013)

[7] P. Lawaetz, Phys. Rev. B**4**, 3460 (1971)

[8] The fits in Fig. 2 are better than reported previously due to the correction of a computational error (erratum to be published). The new set of fitting parameters given in this work are therefore different from those given previously (see Refs. 5 and 6). As previously we have also used α=β=0.2 eV Å (in order to see a spin splitting in the in-plane dispersion due to α) but setting them to zero has almost no effect.

[9] As for the InAs/GaSb T2SLs, values of $\alpha = \beta = 0.2$ eV Å were used for the off diagonal interface parameters, although setting them to zero has almost no effect.

[10] Y. Lin, D. Wang, D. Donets, L. Shterengas, G. Kipshidze, G. Belenky, S.P. Svensson, W.L. Sarney, H.S. Hier, Journ. Electron. Materials **42**, 918 (2013)

[11] Physics of Group IV Elements and III-V Compounds, Landolt-Börnstein New Series, Group III, Vol 17, edited by K.H. Hellwege and O. Madelung, pp. 634-635 (Springer, Berlin 1982)

[12] I. Vurgaftman, J.R. Meyer and L.R. Ram-Mohan, J. Appl. Phys. **89**, 5815 (2001).

[13] R.A. Stradling in *"Growth and Characterisation of Semiconductors"* edited by R.A. Stradling and P.C Klipstein, pp. 165-185 (Adam Hilger, Bristol and New York, 1990)

[14] P.C. Klipstein (2003) *Depletionless Photodiode with Suppressed Dark Current*…, US Patent 7,795,640 (2 July 2003)

[15] P.C. Klipstein (2006) *Unipolar semiconductor photodetector with Suppressed Dark Current*…, US Patent 8,004,012 (6 April 2006)

[16] P.C. Klipstein, Proc. SPIE **6940**, 6940-2U (2008)

[17] P.C. Klipstein, D. Aronov, M. ben Ezra[1], I. Barkai, E. Berkowicz, M. Brumer, R. Fraenkel, A. Glozman, S. Grossman, E. Jacobsohn, O. Klin, I. Lukomsky, L. Shkedy, I. Shtrichman, N. Snapi, M. Yassen, and E. Weiss., IR Physics and Technology **59**, 172 (2013)

[18] H.S. Kim, O.O. Cellek, Zhi-Yuan Lin, Zhao-Yu He, Xin-Hao Zhao, Shi Liu, H. Li and Y.-H. Zhang, Appl. Phys. Lett. **101**, 161114 (2012)

[19] P.C. Klipstein, O. Klin, S. Grossman, N. Snapi, I. Lukomsky, M. Yassen, D. Aronov, E. Berkowicz, A. Glozman, O. Magen, I. Shtrichman, R. Fraenkel and E. Weiss, Proc. SPIE **8268**, 8268-0U (2012)

[20] J. Lekner, Theory of Reflection, (Springer Verlag, Berlin, 1987)

[21] P.C. Klipstein, O. Klin, S. Grossman, N. Snapi, B. Yaakobovitz, M. Brumer, I. Lukomsky, D. Aronov, M. Yassen, B. Yofis, A. Glozman, T. Fishman, E. Berkowicz, O. Magen, I. Shtrichman, and E. Weiss, Proc. SPIE **7608**, 7608-1V (2010)

[22] F. Van de Wiele, Solid State Imaging (Pub. Noordhoff International) p44 (1976)

[23] B.V. Olson, "Time-resolved measurements of charge carrier dynamics and optical nonlinearities in narrow-bandgap semiconductors." dissertation, University of Iowa.(http://ir.uiowa.edu/etd/2596), (2013)

[24] G. Belenky, G. Kipshidze, D. Donetsky, S. P. Svensson, W. L. Sarney, H. Hier, L. Shterengas, D. Wang, and Y. Lin, Proc. SPIE **8012**, 8012-0W (2011)